

## Electronic Supplementary Information

### **$\beta$ -IminoBODIPY oligomers: Facilely accessible $\pi$ -conjugated luminescent BODIPY arrays**

Mizuho Tsuchiya,<sup>a</sup> Ryota Sakamoto,<sup>\*ab</sup> Masaki Shimada,<sup>a</sup> Yoshinori Yamanoi,<sup>a</sup> Yohei Hattori,<sup>a</sup> Kunihisa Sugimoto,<sup>c</sup> Eiji Nishibori<sup>d</sup> and Hiroshi Nishihara<sup>\*a</sup>

<sup>a</sup>Department of Chemistry, Graduate School of Science, The University of Tokyo, 7-3-1, Hongo, Bunkyo-ku, Tokyo 113-0033, Japan

<sup>b</sup>JST-PRESTO, 4-1-8, Honcho, Kawaguchi, Saitama 332-0012, Japan

<sup>c</sup>Japan Synchrotron Radiation Research Institute (JASRI), 1-1-1 Koto, Sayo-cho, Sayo-gun, Hyogo, 679-5198, Japan

<sup>d</sup>Division of Physics, Faculty of Pure and Applied Sciences, Tsukuba Research Center for Interdisciplinary Materials Science (TIMS) & Center for Integrated Research in Fundamental Science and Engineering (CiRFSE), University of Tsukuba, 1-1-1 Tennodai, Tsukuba, Ibaraki, 305-8571, Japan

#### **Contents:**

- A. Experimental
- B. Synthesis of BODIPY **4**
- C. Crystallographic data
- D. IR spectroscopy of BODIPYs
- E. Thermogravimetric analysis of BODIPYs
- F. UV/vis spectroscopy and photophysics of BODIPYs
- G. Electrochemistry
- H. DFT calculation
- I. Photophysical properties of BODIPY-loaded silica gel
- J. References for SI

## A. Experimental

**Materials.** **1**,<sup>S1</sup> **8** (2,6-diiodo-1,3,5,7-tetramethylBODIPY),<sup>S2</sup> and **SG-NH<sub>2</sub>**,<sup>S3</sup> were synthesized according to previous reports. The silica gel for preparing **SG-NH<sub>2</sub>** was purchased from Kanto Chemical Co., Inc. (Cat. No. 37565-85, 60N, spherical,  $\phi = 63 - 210 \mu\text{m}$ , neutral). Tetra-*n*-butylammonium hexafluorophosphate as a supporting electrolyte was purified by recrystallization from ethanol, which was dried in vacuo. Solvents for organic syntheses were purified using a solvent purification system (Ultimate Solvent System, Nikko Hansen & Co., Ltd). The other chemicals were general grades and were used as received. All procedures were conducted under a nitrogen condition otherwise stated.

**Apparatus.** <sup>1</sup>H (500 MHz) and <sup>13</sup>C (125 MHz) nuclear magnetic resonance (NMR) data were collected in CDCl<sub>3</sub> on a Bruker US500 spectrometer. Tetramethylsilane ( $\delta_{\text{H}} = 0.00$ ) was used as an internal standard for the <sup>1</sup>H NMR spectra, and CDCl<sub>3</sub> ( $\delta_{\text{C}} = 77.0$ ) was used as an internal standard for the <sup>13</sup>C NMR spectra, respectively. Fast atom bombardment mass spectrometry (FAB-MS) and electrospray ionization time-of-flight mass spectrometry were conducted using a JEOL JMS-700 MStation and Micromass LCT Premier XE mass spectrometer, respectively. Absorption spectra were measured with a JASCO V-570 spectrometer. Fluorescence spectra were measured with a HITACHI F-4500 spectrometer. Preparative gel permeation liquid chromatography was performed by a LaboACE LC-5060 with JAIGEL H1 + H2 columns (Japan Analytical Industry Co., Ltd.), whose eluent is CHCl<sub>3</sub> at a flow rate of 3.5 mL min<sup>-1</sup>. Absolute fluorescence quantum yields were collected with HAMAMATSU C9920-01. Fluorescence lifetime measurements were performed using a Hamamatsu Photonics Quantaaurus-Tau C11367-02. Thermogravimetric analysis was performed under a nitrogen atmosphere using Rigaku Thermo Plus2 TG8120. Al<sub>2</sub>O<sub>3</sub> was used as a reference compound, and both sample and Al<sub>2</sub>O<sub>3</sub> were mounted on an Al pan. The temperature was controlled from r.t. to 500 °C with a scan rate of 10 °C min<sup>-1</sup>. Electrochemical data were recorded on an ALS 750A Electrochemical analyzer (BAS Co., Ltd.) and a HZ-3000 electrochemical analyzer (Hokuto Denko Co. Ltd.), each equipped with a UNISOKU cryostat. The working electrode was a 0.3 mm o.d. glassy carbon electrode; a platinum wire was used for the auxiliary electrode, and the reference electrode was an Ag<sup>+</sup>/Ag electrode (a silver wire immersed in 0.1 M <sup>n</sup>Bu<sub>4</sub>NClO<sub>4</sub> / 0.01 M AgClO<sub>4</sub> in acetonitrile). Fluorescence microscopic images were obtained using an Olympus BX51 microscope equipped with a U-RFL-T high pressure mercury lamp and WU (UV), WIB (blue), and WIG filters (green), passing through  $\lambda > 420, 510, \text{ and } 575 \text{ nm}$ , respectively.

**Single-crystal X-ray structural analysis.** Single crystals suitable for X-ray diffraction analysis were obtained by vapor diffusion. The solvents used (good / poor) are dichloromethane / methanol for **1**, **6a<sub>2</sub>**, **6c<sub>2</sub>·2CH<sub>3</sub>OH**, **6d<sub>2</sub>**, and **7c<sub>2</sub>**, and dichloromethane / *n*-hexane for **2** and **3**. Synchrotron radiation (SR) X-ray diffraction data of **7c<sub>2</sub>** were collected at 100K. The diffractions were recorded on a CCD detector at SPring-8 beam line BL02B1 (Hyogo, Japan) (SR,  $\lambda = 0.3540 \text{ \AA}$ ).<sup>S4</sup> X-ray diffraction data of **2**, **3**, and **6a<sub>2</sub>** were collected at 93 K on a Rigaku Saturn724 (Varimax dual) diffractometer with multi-layer mirror monochromated MoK $\alpha$  radiation ( $\lambda = 0.71075 \text{ \AA}$ ). X-ray diffraction data of **1**, **6c<sub>2</sub>·2CH<sub>3</sub>OH**, and **6d<sub>2</sub>** were collected at 113 K with an AFC10 diffractometer coupled with a Rigaku Saturn CCD system equipped with a rotating-anode X-ray

generator producing graphite-monochromated MoK $\alpha$  radiation ( $\lambda = 0.7107 \text{ \AA}$ ). The structures were solved by direct methods using SIR-92 program<sup>SSa</sup> (**3**, **6c<sub>2</sub>**·**2CH<sub>3</sub>OH**, and **7c<sub>2</sub>**) or SIR-2004 program<sup>SSb</sup> (**1**, **2**, **6a<sub>2</sub>**, and **6d<sub>2</sub>**) and refined by the full-matrix least-squares techniques against  $F^2$  implementing SHELXL97.<sup>SSc</sup> Crystallographic data for the structure of **1**, **2**, **3**, **6a<sub>2</sub>**, **6c<sub>2</sub>**·**2CH<sub>3</sub>OH**, **6d<sub>2</sub>**, and **7c<sub>2</sub>** have been deposited with the Cambridge Crystallographic Data Centre as supplementary publication nos. CCDC 1527793, 1527794, 1527795, 1527723, 1527810, 1527797 and 1527798.

**DFT calculation methods.** Compounds **6a<sub>2</sub>**, **6c<sub>2</sub>**, **6d<sub>2</sub>**, **7c<sub>2</sub>**, **7c<sub>3</sub>**, and **7c<sub>4</sub>** were modeled with the Gaussian 09 suite of programs using the density functional theory (DFT). The  $S_0$  geometry optimization was conducted with B3LYP/6-31G(d) for **6a<sub>2</sub>**, **6c<sub>2</sub>**, **6d<sub>2</sub>**, **7c<sub>2</sub>**, **7c<sub>3</sub>**, and **7c<sub>4</sub>** for the ground state without solvation. It was confirmed that the optimized geometry does not contain any imaginary frequencies.

**Synthesis of 2.** Phosphoryl chloride (4 mL) was slowly added to *N,N*-dimethylformamide (4 mL) at 0 °C. BODIPY **1** (2.22 g, 6.06 mmol) in chloroform (20 mL) was added to the solution. The mixture was heated and stirred at 50 °C for 60 min. After confirming the consumption of the starting material on TLC, the solution was cooled to room temperature, diethyl ether (100 mL) was added and poured into NaHCO<sub>3</sub>aq. The organic layer was washed with water and dried over MgSO<sub>4</sub>. After filtration, the crude material was purified by reprecipitation from diethyl ether/methanol. Yield: 1.91g (80%), orange powder. <sup>1</sup>H NMR (500 MHz, CDCl<sub>3</sub>):  $\delta$  = 10.01 (s, 1H), 6.99 (s, 2H), 6.14 (s, 1H), 2.83 (s, 3H), 2.62 (s, 3H), 2.36 (s, 3H), 2.09 (s, 6H), 1.69 (s, 3H), 1.42 (s, 3H); <sup>13</sup>C NMR (125 MHz, CDCl<sub>3</sub>):  $\delta$  = 185.9, 161.3, 156.3, 146.5, 143.8, 142.0, 139.3, 134.7, 133.5, 130.3, 129.3, 128.8, 126.1, 123.6, 21.2, 19.5, 15.1, 13.9, 13.0, 10.4; FT-IR (KBr, cm<sup>-1</sup>): 2914, 2860, 2769, 1676, 1610, 1547, 1471, 1414, 1319, 1254, 1194, 1113, 1084, 1018, 978, 856, 816, 704, 521; HR-FAB-MS ( $m/z$ ): [M]<sup>+</sup>, calculated for C<sub>23</sub>H<sub>25</sub>ON<sub>2</sub>F<sub>2</sub>B<sup>+</sup>, 394.2028, found, 394.2015.

**Synthesis of 3.** Phosphoryl chloride (4 mL) was slowly added to *N,N*-dimethylformamide (4 mL) at 0 °C. BODIPY **1** (395 mg, 1.00 mmol) in chloroform (20 mL) was added to the solution. The mixture was heated and stirred at 60 °C for 3 hours. After confirming the consumption of the starting material on TLC, the solution was cooled to room temperature and poured into an aqueous solution of K<sub>2</sub>CO<sub>3</sub>. The organic layer was washed with water and dried over MgSO<sub>4</sub>. After filtration, the solvent was removed and the crude material was purified by column chromatography (SiO<sub>2</sub>, eluent: dichloromethane). Yield: 320 mg (76%), red powder. <sup>1</sup>H NMR (500 MHz, CDCl<sub>3</sub>):  $\delta$  = 10.07 (s, 2H), 7.04 (s, 2H), 2.89 (s, 6H), 2.38 (s, 3H), 2.09 (s, 6H), 1.75 (s, 6H); <sup>13</sup>C NMR (125 MHz, CDCl<sub>3</sub>):  $\delta$  = 185.6, 160.5, 148.0, 147.5, 140.0, 134.3, 131.1, 129.8, 129.7, 127.8, 21.2, 19.5, 13.7, 10.9; FT-IR (KBr, cm<sup>-1</sup>): 2968, 2918, 2856, 2750, 1678, 1610, 1525, 1502, 1475, 1408, 1311, 1250, 1200, 1174, 1134, 1088, 1009, 862, 777, 752, 700, 519, 418; HR-FAB-MS ( $m/z$ ): [M]<sup>+</sup>, calculated for C<sub>23</sub>H<sub>25</sub>ON<sub>2</sub>F<sub>2</sub>B<sup>+</sup>, 422.1977, found, 422.2004.

**Synthesis of 4.** The synthetic route is shown in Scheme S1. Triethylamine (30 mL) was bubbled with nitrogen for 25 min before **8**<sup>86</sup> (610 mg, 0.987 mmol), 4-ethynylbenzaldehyde (330 mg, 2.54 mmol), copper iodide (15 mg, 79  $\mu$ mol), and bis(triphenylphosphine)palladium(II) dichloride (37 mg, 53  $\mu$ mol) were added and heated to 50 °C overnight. The reaction mixture was cooled to room temperature and the solvent was removed. The residue was purified by column chromatography (aluminum oxide, dichloromethane). The pink

band was collected and evaporated. The crude material was reprecipitated from methanol/dichloromethane. Yield: 0.519 g (83%), purple powder.  $^1\text{H}$  NMR (500 MHz,  $\text{CDCl}_3$ ):  $\delta$  = 10.00 (s, 2H), 7.84 (d,  $J$  = 8.5 Hz, 4H), 7.59 (d,  $J$  = 8.5 Hz, 4H), 2.75 (s, 6H), 2.38 (s, 3H), 2.11 (s, 6H), 1.57 (s, 6H);  $^{13}\text{C}$  NMR (125 MHz,  $\text{CDCl}_3$ ):  $\delta$  = 191.3, 158.6, 144.0, 143.4, 139.4, 135.2, 134.7, 131.7, 130.6, 130.3, 129.7, 129.6, 129.3, 115.3, 95.9, 86.1, 21.2, 19.5, 13.8, 12.4; HR-FAB-MS ( $m/z$ ):  $[\text{M}+\text{H}]^+$ , calculated for  $\text{C}_{40}\text{H}_{34}\text{BF}_2\text{N}_2\text{O}_s^+$ , 623.2676; found, 623.2676.

**Synthesis of 6a<sub>2</sub>.** Ethylenediamine (10  $\mu\text{L}$ , 0.15 mmol) and **2** (78 mg, 0.20 mmol) were allowed to react with each other in dichloromethane (10 mL) at room temperature for 24 h. The residue was reprecipitated from dichloromethane / methanol to give the pure product. Yield: 65 mg (80%), brown powder.  $^1\text{H}$  NMR (500 MHz,  $\text{CDCl}_3$ ):  $\delta$  = 8.23 (s, 2H), 6.95 (s, 4H), 6.01 (s, 2H), 3.79 (s, 4H), 2.73 (s, 6H), 2.57 (s, 6H), 2.33 (s, 6H), 2.06 (s, 12H), 1.53 (s, 6H), 1.38 (s, 6H);  $^{13}\text{C}$  NMR (125 MHz,  $\text{CDCl}_3$ ):  $\delta$  = 157.2, 155.9, 155.4, 143.8, 142.6, 140.6, 138.8, 134.8, 131.6, 130.9, 129.5, 129.1, 125.4, 121.8, 63.2, 21.2, 19.5, 14.8, 13.8, 13.6, 10.8; FT-IR (KBr,  $\text{cm}^{-1}$ ): 2972, 2920, 2846, 2733, 2364, 2339, 1633, 1610, 1539, 1510, 1475, 1439, 1308, 1255, 1225, 1200, 1188, 1163, 1113, 1090, 1063, 1030, 984, 854, 810, 775, 756, 706, 646, 582, 540, 492; HR-FAB-MS ( $m/z$ ):  $[\text{M}]^+$ , calculated for  $\text{C}_{48}\text{H}_{54}\text{N}_6\text{F}_4\text{B}_2^+$ , 812.4532; found, 812.4527.

**Synthesis of 6b<sub>2</sub>.** 1,12-dodecanediamine (40 mg, 0.20 mmol) and **2** (203 mg, 0.511 mmol) were allowed to react with each other in dichloromethane (10 mL) at room temperature for 24 h. The solvent was removed from the reaction mixture and processed on GPC to give the pure product. Yield: 60 mg (25%), orange solid.  $^1\text{H}$  NMR (500 MHz,  $\text{CDCl}_3$ ):  $\delta$  = 8.25 (s, 2H), 6.95 (s, 4H), 6.01 (s, 2H), 3.49 (t,  $J$  = 6.9 Hz, 4H), 2.78 (s, 6H), 2.57 (s, 6H), 2.34 (s, 6H), 2.09 (s, 12H), 1.61 – 1.59 (m, 10H), 1.38 (s, 6H), 1.36 – 1.22 (m, 16H);  $^{13}\text{C}$  NMR (125 MHz,  $\text{CDCl}_3$ ):  $\delta$  = 157.0, 155.5, 154.1, 143.6, 142.5, 140.6, 138.8, 134.9, 131.6, 131.0, 129.6, 129.1, 125.6, 121.7, 63.0, 31.4, 29.6, 29.6, 29.4, 27.3, 21.2, 19.5, 14.7, 13.7, 13.6, 10.9; HR-FAB-MS ( $m/z$ ):  $[\text{M}+\text{H}]^+$ , calculated for  $\text{C}_{58}\text{H}_{75}\text{N}_6\text{F}_4\text{B}_2^+$ , 953.6175; found, 953.6156.

**Synthesis of 6c<sub>2</sub>.** Hydrazine monohydrate (9.0  $\mu\text{L}$ , 0.15 mmol) and **2** (79 mg, 0.20 mmol) were allowed to react with each other in dichloromethane (10 mL) at room temperature for 24 h. The residue was reprecipitated from dichloromethane / methanol to give the pure product. Yield: 67 mg (85%), brown powder.  $^1\text{H}$  NMR (500 MHz,  $\text{CDCl}_3$ ):  $\delta$  = 8.60 (s, 2H), 6.97 (s, 4H), 6.04 (s, 2H), 2.85 (s, 6H), 2.59 (s, 6H), 2.34 (s, 6H), 2.09 (s, 12H), 1.63 (s, 6H), 1.40 (s, 6H);  $^{13}\text{C}$  NMR (125 MHz,  $\text{CDCl}_3$ ):  $\delta$  = 157.8, 155.7, 155.2, 144.3, 142.5, 140.6, 138.9, 134.9, 131.9, 130.8, 129.8, 129.1, 123.4, 122.2, 21.2, 19.5, 14.8, 14.12, 13.7, 11.3; FT-IR (KBr,  $\text{cm}^{-1}$ ): 2974, 2924, 2856, 2735, 2362, 2343, 1618, 1537, 1508, 1464, 1410, 1362, 1308, 1252, 1188, 1163, 1115, 1070, 1014, 982, 881, 854, 816, 779, 739, 704, 631, 584, 559, 523, 480; HR-FAB-MS ( $m/z$ ):  $[\text{M}]^+$ , calculated for  $\text{C}_{46}\text{H}_{50}\text{N}_6\text{F}_4\text{B}_2^+$ , 784.4219, found, 784.4211.

**Synthesis of 6d<sub>2</sub>.** 1,4-phenylenediamine (16 mg, 0.15 mmol) and **2** (79 mg, 0.20 mmol) were allowed to react with each other in dichloromethane (10 mL) at room temperature for 2 h. The residue was reprecipitated from dichloromethane / methanol to give the pure product. Yield: 37 mg (43%), brown powder.  $^1\text{H}$  NMR (500 MHz,  $\text{CDCl}_3$ ):  $\delta$  = 8.64 (s, 2H), 7.12 (s, 4H), 6.98 (s, 4H), 6.06 (s, 4H), 2.90 (s, 6H), 2.60 (s, 6H), 2.35 (s, 6H), 2.11 (s, 12H), 1.69 (s, 6H), 1.40 (s, 6H);  $^{13}\text{C}$  NMR (125 MHz,  $\text{CDCl}_3$ ):  $\delta$  = 156.0, 153.1, 150.8, 144.4,

142.8, 141.0, 138.9, 134.9, 132.1, 130.9, 129.6, 129.2, 125.5, 122.3, 121.5, 115.6, 21.2, 19.5, 14.9, 14.0, 13.7, 11.0; FT-IR (KBr,  $\text{cm}^{-1}$ ): 2918, 2858, 1610, 1535, 1362, 1308, 1254, 1219, 1186, 1163, 1018, 982, 893, 850, 808, 702; HR-FAB-MS ( $m/z$ ):  $[\text{M}]^+$ , calculated for  $\text{C}_{52}\text{H}_{54}\text{N}_6\text{F}_4\text{B}_2^+$ , 860.4532; found, 860.4542.

**Synthesis of 7a(m) and 7a3-r.** 1,2-ethylenediamine (5.3  $\mu\text{L}$ , 0.080 mmol) and **3** (86 mg, 0.20 mmol) were allowed to react with each other in dichloromethane (10 mL) at room temperature for 3 h. The solvent was evaporated and the residue was processed on GPC, such that **7a3-r** was isolated. Yield: 12 mg (14%), red powder.  $^1\text{H}$  NMR (500 MHz,  $\text{CDCl}_3$ ):  $\delta$  = 8.10 (s, 6H), 6.92 (s, 6H), 3.85 (s, 12H), 2.66 (s, 18H), 2.20 (s, 9H), 1.96 (s, 18H), 1.45 (s, 18H);  $^{13}\text{C}$  NMR (125 MHz,  $\text{CDCl}_3$ ):  $\delta$  = 157.0, 156.1, 143.8, 142.0, 139.0, 134.6, 130.6, 130.5, 129.2, 126.2, 62.3, 20.9, 19.4, 13.7, 11.0; FT-IR (KBr,  $\text{cm}^{-1}$ ): 2920, 2835, 2731, 1639, 1610, 1533, 1473, 1437, 1358, 1315, 1257, 1209, 1186, 1092, 1043, 1011, 968, 910, 852, 781, 754, 731, 706, 592, 544; HR-ESI-MS ( $m/z$ ):  $[\text{M}+\text{H}]^+$ , calculated for  $\text{C}_{78}\text{H}_{87}\text{B}_3\text{F}_6\text{N}_{12}^+$ , 1339.7471; found, 1339.7415.

**Synthesis of 7b(m).** 1,12-dodecanediamine (16 mg, 0.080 mmol) and **3** (84 mg, 0.20 mmol) were allowed to react with each other in dichloromethane (10 mL) at room temperature for 3 h. The solvent was evaporated and the residue was processed on GPC, however, no purified material was isolated.

**Synthesis of 7c(m) and 7c<sub>n</sub> (n = 2–6).** Hydrazine monohydrate (9.0  $\mu\text{L}$ , 0.18 mmol) and **3** (85 mg, 0.20 mmol) were allowed to react with each other in dichloromethane (10 mL) at room temperature for 3 h. The solvent was evaporated and the residue was processed on GPC to isolate five oligomers, **7c<sub>n</sub>** ( $n = 2–6$ ).

**Identification of 7c<sub>2</sub>.** Yield: 23.8 mg (28.2%), purple powder.  $^1\text{H}$  NMR (500 MHz,  $\text{CDCl}_3$ ):  $\delta$  = 10.05 (s, 2H), 8.60 (s, 2H), 7.01 (s, 4H), 2.92 (s, 6H), 2.86 (s, 6H), 2.37 (s, 6H), 2.10 (s, 12H), 1.71 (s, 6H), 1.65 (s, 6H);  $^{13}\text{C}$  NMR (125 MHz,  $\text{CDCl}_3$ ):  $\delta$  = 185.8, 161.1, 158.2, 155.1, 145.5, 145.0, 144.6, 139.7, 134.6, 132.4, 130.2, 129.9, 129.5, 125.9, 125.8, 21.2, 19.5, 15.1, 13.4, 11.6, 10.6; HR-FAB-MS ( $m/z$ ):  $[\text{M}+\text{H}]^+$ , calculated for  $\text{C}_{48}\text{H}_{51}\text{B}_2\text{F}_4\text{N}_6\text{O}_2^+$ , 841.4196; found, 841.4188.

**Identification of 7c<sub>3</sub>.** Yield: 11.1 mg (13.1%), purple powder.  $^1\text{H}$  NMR (500 MHz,  $\text{CDCl}_3$ ):  $\delta$  = 10.04 (s, 2H), 8.61 (s, 2H), 8.59 (s, 2H), 7.01 (s, 4H), 7.00 (s, 2H), 2.93 (s, 6H), 2.90 (s, 6H), 2.86 (s, 6H), 2.37 (s, 6H), 2.36 (s, 3H), 2.10 (s, 6H), 2.09 (s, 12H), 1.71 (s, 6H), 1.65 (s, 6H), 1.64 (s, 6H);  $^{13}\text{C}$  NMR (125 MHz,  $\text{CDCl}_3$ ):  $\delta$  = 185.8, 161.2, 158.3, 158.0, 155.7, 154.5, 145.4, 144.8, 144.4, 143.9, 142.9, 139.6, 139.4, 134.8, 134.6, 132.4, 131.1, 130.5, 130.2, 129.8, 129.5, 129.4, 126.8, 126.1, 124.5, 21.2, 19.5, 19.5, 15.1, 14.6, 13.3, 11.6, 11.5, 10.6, 8.1; HR-ESI-MS:  $[\text{M}+\text{H}]^+$ , calculated for:  $\text{C}_{72}\text{H}_{76}\text{B}_3\text{F}_6\text{N}_{10}\text{O}_2^+$ , 1258.6343, found, 1258.6385.

**Identification of 7c<sub>4</sub>.** Yield: 5.2 mg (6.2%), purple powder.  $^1\text{H}$  NMR (500 MHz,  $\text{CDCl}_3$ ):  $\delta$  = 10.04 (s, 2H), 8.61 (s, 2H), 8.60 (s, 2H), 8.59 (s, 2H), 7.01 (s, 4H), 7.00 (s, 4H), 2.93 (s, 6H), 2.89 (s, 12H), 2.86 (s, 6H), 2.37 (s, 6H), 2.36 (s, 6H), 2.10 (s, 12H), 2.09 (s, 12H), 1.71 (s, 6H), 1.65 (s, 6H), 1.64 (s, 12H); HR-ESI-MS:  $[\text{M}+\text{H}]^+$ , calculated for:  $\text{C}_{96}\text{H}_{101}\text{B}_4\text{F}_8\text{N}_{14}\text{O}_2^+$ , 1677.8523, found, 1677.8511;  $^{13}\text{C}$  NMR not obtained due to low solubility.

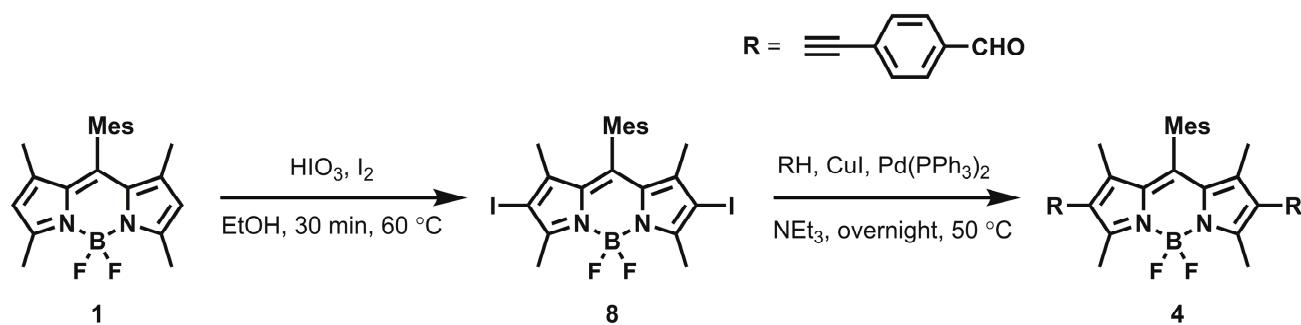
**Identification of 7c<sub>5</sub>.** Yield: 2.3 mg (2.7%), purple powder.  $^1\text{H}$  NMR (500 MHz,  $\text{CDCl}_3$ ):  $\delta$  = 10.04 (s, 2H), 8.61 (s, 2H), 8.60 (s, 4H), 8.59 (s, 2H), 7.01 (s, 4H), 7.00 (s, 4H), 2.93 (s, 6H), 2.89 (s, 18H), 2.86 (s, 6H), 2.37 (s, 6H), 2.36 (s, 6H), 2.10 (s, 12H), 2.09 (s, 12H), 1.71 (s, 6H), 1.65 (s, 6H), 1.64 (s, 18H); HR-

ESI-MS:  $[M+H]^+$ , calculated for:  $C_{120}H_{126}B_5F_{10}N_{18}O_2^+$ , 2095.0679, found, 2095.0679;  $^{13}C$  NMR not obtained due to low solubility.

**Identification of 7c<sub>6</sub>.** Yield: 1.3 mg (1.5%), purple powder.  $^1H$  NMR (500 MHz,  $CDCl_3$ ):  $\delta$  = 10.04 (s, 2H), 8.61 (s, 2H), 8.60 (s, 6H), 8.59 (s, 2H), 7.01 (s, 4H), 6.99 (s, 8H), 2.93 (s, 6H), 2.89 (s, 24H), 2.86 (s, 6H), 2.37 (s, 6H), 2.36 (s, 12H), 2.10 (s, 18H), 2.09 (s, 18H), 1.71 (s, 6H), 1.65 (s, 6H), 1.64 (s, 24H); HR-ESI-MS:  $[M+H]^+$ , calculated for:  $C_{144}H_{151}B_6F_{12}N_{22}O_2^+$ , 2514.2803, found, 2514.2837;  $^{13}C$  NMR not obtained due to low solubility.

**Preparation of BODIPY-loaded silica gel.** Amino-group terminated silica gel was prepared according to a reported method using neutral spherical silica gel whose diameter spans 63 – 210  $\mu m$ .<sup>25</sup> To 1.0 g the silica gel, a  $1.0 \times 10^{-4}$  mol  $L^{-1}$  solution (10 mL, in dichloromethane) of **3** or **4** was reacted on a shaker overnight. The silica gel was filtered, rinsed with methanol and vacuum drying after the reaction to obtain  $1.0 \times 10^{-6}$  mol  $g^{-1}$  loaded silica gel samples (**SG-NH<sub>2</sub>-3** and **SG-NH<sub>2</sub>-4**). Note that during the filtration and rinsing processes after the reaction, there was no obvious elution of BODIPY off the silica gel. Along with the chemically-bonded samples, as reference samples, **SG-OH-1**, **SG-NH<sub>2</sub>-1**, and **SG-OH-3** were also prepared by immersing 1.0 g of silica gel in a dichloromethane solution ( $1.0 \times 10^{-4}$  mol  $L^{-1}$ , 10 mL) of **1** or **3**, followed by evaporation of the solvent and vacuum drying.

## B. Synthesis of BODIPY 4



**Scheme S1.** The synthesis of BODIPY **4** via BODIPY **8**.

### C. Crystallographic data

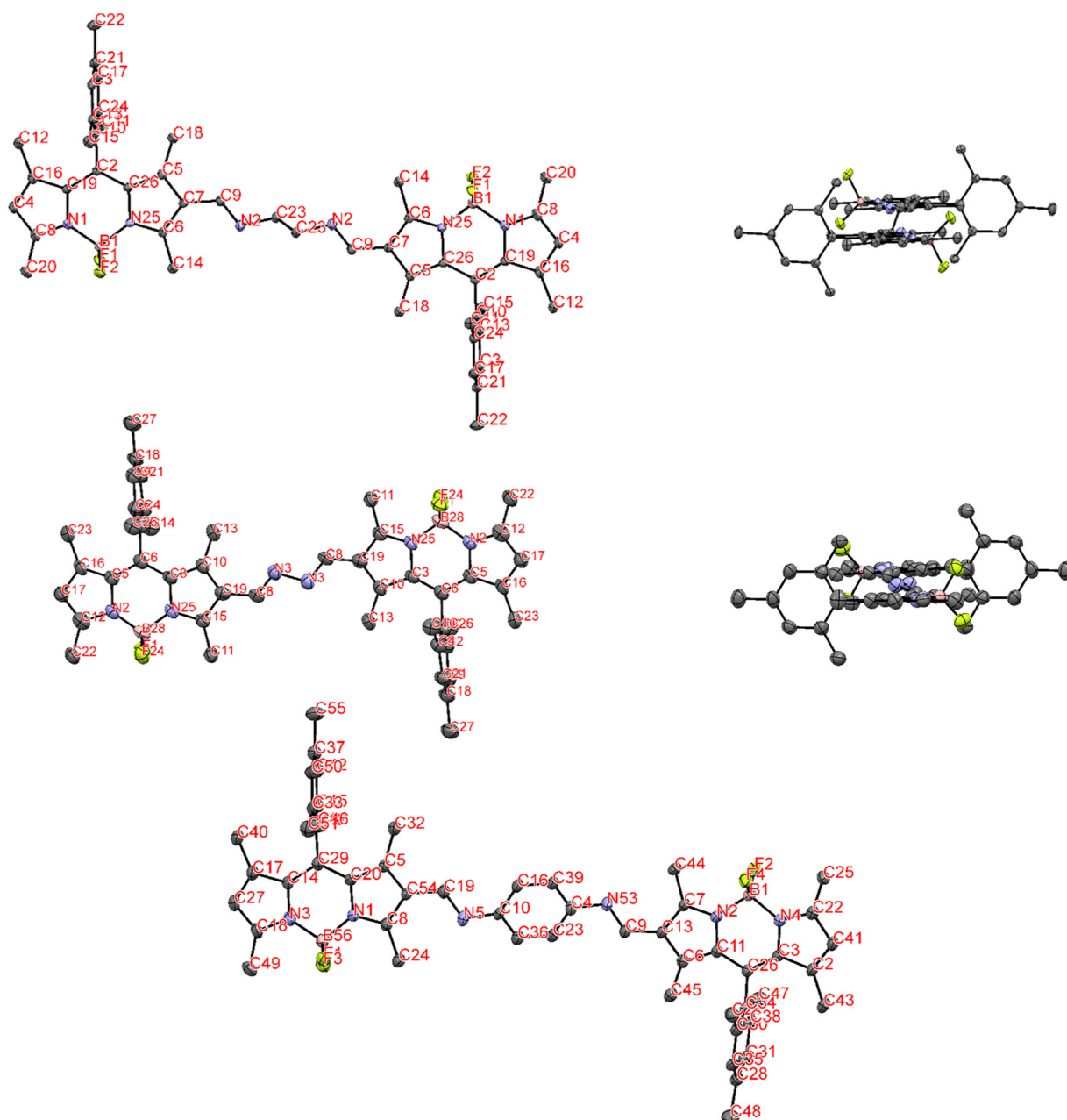


**Fig. S1.** ORTEP drawings of imine-tethered BODIPY dimers **6a<sub>2</sub>** (top), **6c<sub>2</sub>·2CH<sub>3</sub>OH** (middle), and **6d<sub>2</sub>** (bottom) with thermal ellipsoids set at the 50% probability level. Gray, carbon; red, oxygen; blue, nitrogen; green, zinc. Hydrogen atoms and crystal solvent molecules are omitted for clarity. In **6a<sub>2</sub>**, The C=N (C9–N2) bond length is 1.269(2) Å. The N–CH<sub>2</sub> (N2–C9) and CH<sub>2</sub>–CH<sub>2</sub> (C23–C23) lengths are 1.463(2) Å and 1.515(3) Å, respectively, typical bond lengths for each species. The two dipyrrole planes interconnected by the ethylenediamine bond are virtually parallel, whose interplanar distance is 0.665 Å. In **6c<sub>2</sub>·2CH<sub>3</sub>OH**, the N–N (N3–N3) bond length is 1.444(8) Å and the C=N (C8–N3) length is 1.296(10) Å. The interplanar distance of the two dipyrrole is 1.019 Å. In **6d<sub>2</sub>**, the C=N bond lengths of C9–N53 and C19–N5 are 1.272(5) and 1.291(5) Å, respectively. The angle of the dipyrrole plane (N3, B56, N1, C8, C54, C5, C20, C29, C14, C17, C27, C18) and phenylene moiety (C4, C39, C16, C10, C36, C23) is tilted by 40.51°.

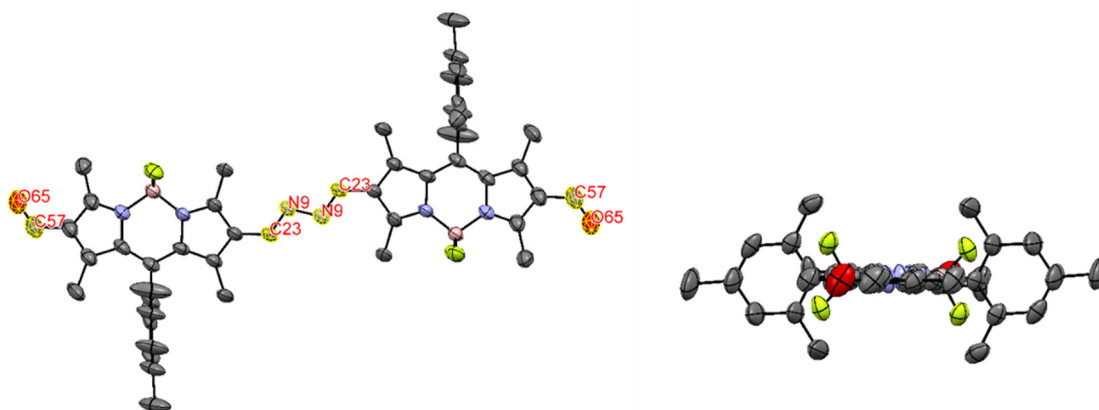


**Fig. S2.** ORTEP drawing of imine-tethered BODIPY dimer **7c<sub>2</sub>** with thermal ellipsoids set at the 50% probability level. Gray, carbon; red, oxygen; blue, nitrogen; green, zinc. Hydrogen atoms and crystal solvent molecules are omitted for clarity. **7c<sub>2</sub>** shows similar bond lengths to **6c<sub>2</sub>·2CH<sub>3</sub>OH**, whose N–N (N9–N9) bond length is 1.402(5) Å and the C=N (C23–N9) length is 1.294(6) Å. The C=O (C57–O65) length is 1.219(7) Å.

**Table S1.** Crystallographic data for **6a<sub>2</sub>**, **6c<sub>2</sub>·2CH<sub>3</sub>OH**, **6d<sub>2</sub>**, and **7c<sub>2</sub>**

	BODIPY <b>6a<sub>2</sub></b>	BODIPY <b>6c<sub>2</sub>·2CH<sub>3</sub>OH</b>	BODIPY <b>6d<sub>2</sub></b>	BODIPY <b>7c<sub>2</sub></b>
Formula	C <sub>48</sub> H <sub>54</sub> B <sub>2</sub> F <sub>4</sub> N <sub>6</sub>	C <sub>46</sub> H <sub>50</sub> B <sub>2</sub> F <sub>4</sub> N <sub>6</sub> ·2C H <sub>3</sub> OH	C <sub>52</sub> H <sub>54</sub> B <sub>2</sub> F <sub>4</sub> N <sub>6</sub>	C <sub>48</sub> H <sub>50</sub> B <sub>2</sub> F <sub>4</sub> N <sub>6</sub> O <sub>2</sub>
Formula Weight	812.61	762.56	860.65	840.58
Crystal System	monoclinic	monoclinic	monoclinic	triclinic
Space Group	<i>P</i> 2 <sub>1</sub> / <i>c</i>	<i>P</i> 2 <sub>1</sub> / <i>n</i>	<i>P</i> 2 <sub>1</sub> / <i>c</i>	<i>Pbca</i>
<i>a</i> (Å)	8.455(3)	11.130(15)	16.986(7)	11.604(3)
<i>b</i> (Å)	11.938(5)	11.266(14)	12.115(5)	12.326(3)
<i>c</i> (Å)	20.565(8)	18.32(3)	21.755(10)	16.967(4)
<i>α</i> (deg)	90	90	90	89.795(10)
<i>β</i> (deg)	92.164(5)	95.019(4)	92.081(7)	70.935(8)
<i>γ</i> (deg)	90	90	90	73.944(8)
<i>V</i> (Å <sup>3</sup> )	2074.3(14)	2288(6)	4474(4)	2194.1(19)
<i>Z</i>	2	2	4	2
Density (g cm <sup>-3</sup> )	1.301	1.107	1.278	1.272
<i>F</i> (000)	860	848	1816	884
Data/Restraints/Parameters	4561/0/271	4996/0/262	10191/0/577	10024/0/578
Goodness of Fit on <i>F</i> <sup>2</sup>	1.09	1.267	0.993	1.023
<i>R</i> <sub>1</sub> ( <i>I</i> > 2σ( <i>I</i> ))	0.0515	0.1534	0.0965	0.0901
w <i>R</i> <sub>2</sub> (all data)	0.1245	0.4332	0.2929	0.2973

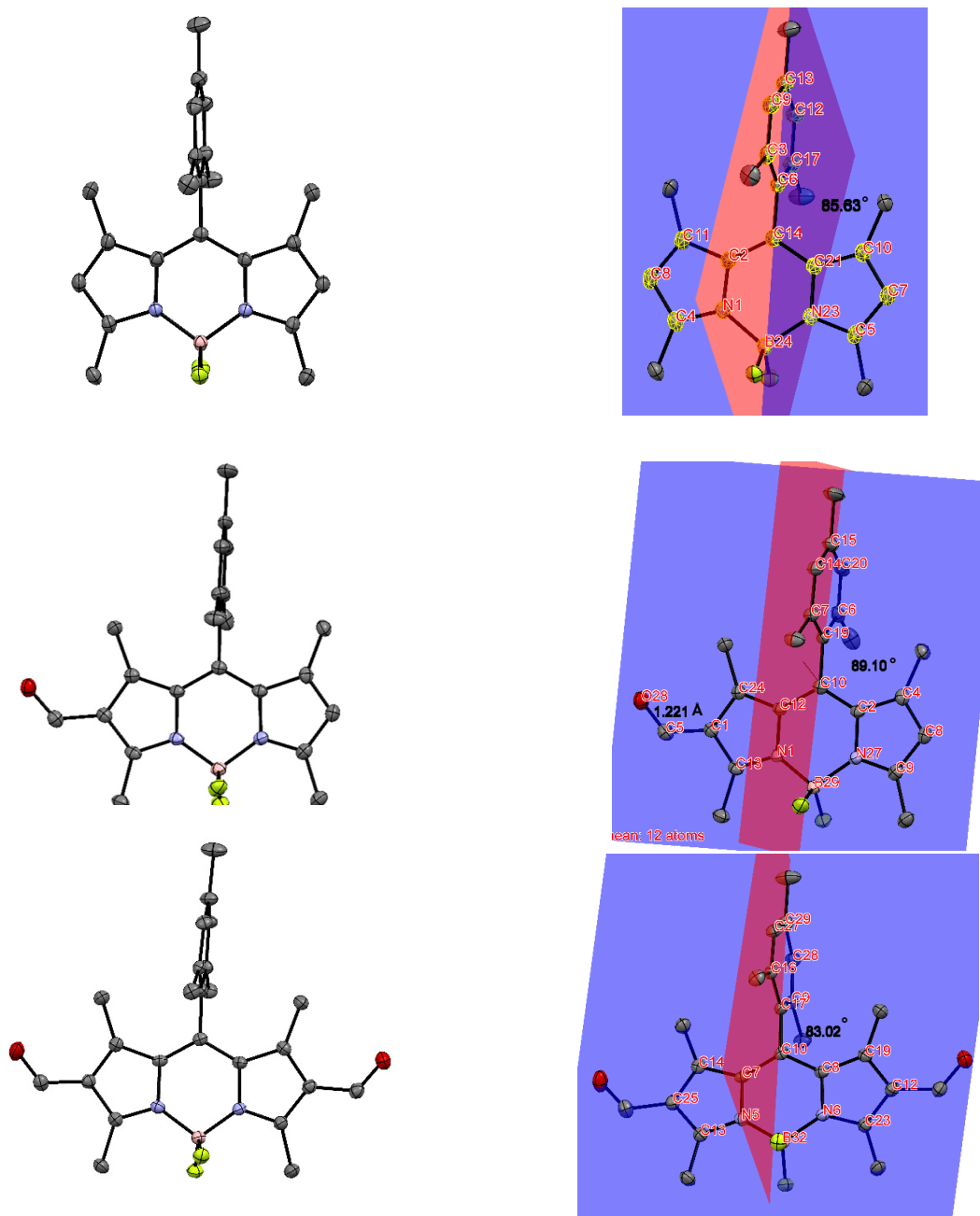


**Fig. S3.** ORTEP drawings of BODIPY precursors **1** (top), **2** (middle), and **3** (bottom). Thermal ellipsoids set at the 50% probability level. Gray, carbon; red, oxygen; purple, nitrogen; pink, boron, yellow green; fluorine. Hydrogen atoms are omitted for clarity. In the crystal structure of **1**, the mesityl group (C6, C17, C12, C13, C5, C3) is virtually orthogonal to the dipyrin core (C14, C21, C10, C7, C5, N23, B24, N1, C4, C8, C11, C2), with a dihedral angle of 85.63°. Similarly, that of **2** (C19, C6, C20, C15, C14, C7) is virtually orthogonal to the dipyrin core (C10, C2, C4, C8, C9, N27, B29, N1, C13, C1, C24, C12), with a dihedral angle of 89.10°. The C=O length of the 2-formyl group (C5, C28) is 1.221(3) Å. In **3**, the mesityl group (C17, C9, C28, C29, C21, C15) is practically orthogonal to the dipyrin core (C10, C6, C19, C12, C23, N6, B32, N5, C13, C25, C14, C7), with a dihedral angle of 83.02°. The C=O lengths (C20–O4, C15–O3) are 1.221(3) and 1.216(3) Å, which are typical of aromatic aldehydes as well.

**Table S2.** Crystallographic data for **1**, **2**, and **3**

	BODIPY <b>1</b>	BODIPY <b>2</b>	BODIPY <b>3</b>
Formula	C <sub>22</sub> H <sub>25</sub> BF <sub>2</sub> N <sub>2</sub>	C <sub>23</sub> H <sub>25</sub> BF <sub>2</sub> N <sub>2</sub> O	C <sub>24</sub> H <sub>25</sub> BF <sub>2</sub> N <sub>2</sub> O <sub>2</sub>
Formula Weight	366.26	394.27	422.28
Crystal System	orthorhombic	orthorhombic	monoclinic
Space Group	<i>P</i> 2 <sub>1</sub> 2 <sub>1</sub> 2 <sub>1</sub>	<i>P</i> bca	<i>P</i> 2 <sub>1</sub> / <i>c</i>
<i>a</i> (Å)	7.799(2)	12.085(3)	15.356(6)
<i>b</i> (Å)	13.378(4)	13.471(4)	8.430(3)
<i>c</i> (Å)	19.206(5)	25.017(7)	17.216(7)
<i>α</i> (deg)	90	90	90
<i>β</i> (deg)	90	90	108.360(4)
<i>γ</i> (deg)	90	90	90
<i>V</i> (Å <sup>3</sup> )	2003.8(9)	4072.7(19)	2115(12)
<i>Z</i>	4	8	4
Density (g cm <sup>-3</sup> )	1.286	1.286	1.326
<i>F</i> (000)	776	1664	888
Data/Restraints/Parameters	4380/0/244	4654/0/262	4790/0/281
Goodness of Fit on <i>F</i> <sup>2</sup>	1.214	1.127	1.123
<i>R</i> <sub>1</sub> ( <i>l</i> > 2σ( <i>l</i> ))	0.0331	0.0607	0.0732
w <i>R</i> <sub>2</sub> (all data)	0.0918	0.1451	0.1641

### Notes for single-crystal X-ray structural analysis.

Single crystals of **1**, **2**, **3**, **6a<sub>2</sub>**, **6c<sub>2</sub>·2CH<sub>3</sub>OH**, **6d<sub>2</sub>**, and **7c<sub>2</sub>** suitable for X-ray single crystal structural analysis were obtained by recrystallization from rich and poor solvents. ORTEP drawings for **6a<sub>2</sub>**, **6c<sub>2</sub>·2CH<sub>3</sub>OH**, and **7c<sub>2</sub>** are shown in Figures 1, S1, and S2, whereas those of **1**, **2**, and **3** are depicted in Figure S3. Their crystallographic data are summarized in Tables S1 and S2. **6a<sub>2</sub>**, the ethylenediimine bridged dimer, possesses bond lengths of 1.269(2), 1.463(2), and 1.515(3) Å, respectively, for C=N (C9–N2), N–CH<sub>2</sub> (N2–C23), and CH<sub>2</sub> – CH<sub>2</sub> (C23–C23). The C=N length is longer than the C=O length in **2** (1.221(3) Å, Fig. S2). The BODIPY planes are not coplanar, whose interplanar distance is 0.665 Å. In **6c<sub>2</sub>·2CH<sub>3</sub>OH**, C=N (C8–N3) and N–N (N3–N3) bond lengths are 1.296(10) and 1.444(8) Å, respectively. The interplanar distance of the two BODIPY subunits is 1.019 Å. **6d<sub>2</sub>** shows C=N lengths of 1.272(5) Å for C9–N53 and 1.291(5) Å for C19–N5. The BODIPY core and the phenylene moiety are tilted with a dihedral angle of 40.51°. **7c<sub>2</sub>**'s structure is similar to **6c<sub>2</sub>·2CH<sub>3</sub>OH**'s structure, whose C=N (C23–N9) length is 1.294(6) Å and

the N–N (N9–N9) bond length is 1.402(5) Å. Its C=N length is longer than the C=O lengths of **3** (1.221(3) and 1.216(3) Å, Fig. S2). **7c<sub>2</sub>**'s C=O (C57–O65) length is 1.219(7) Å, comparable to those of **3**. The bond lengths obtained are consistent with analogous structures.<sup>S7,S8</sup>

D. IR spectroscopy of BODIPYs

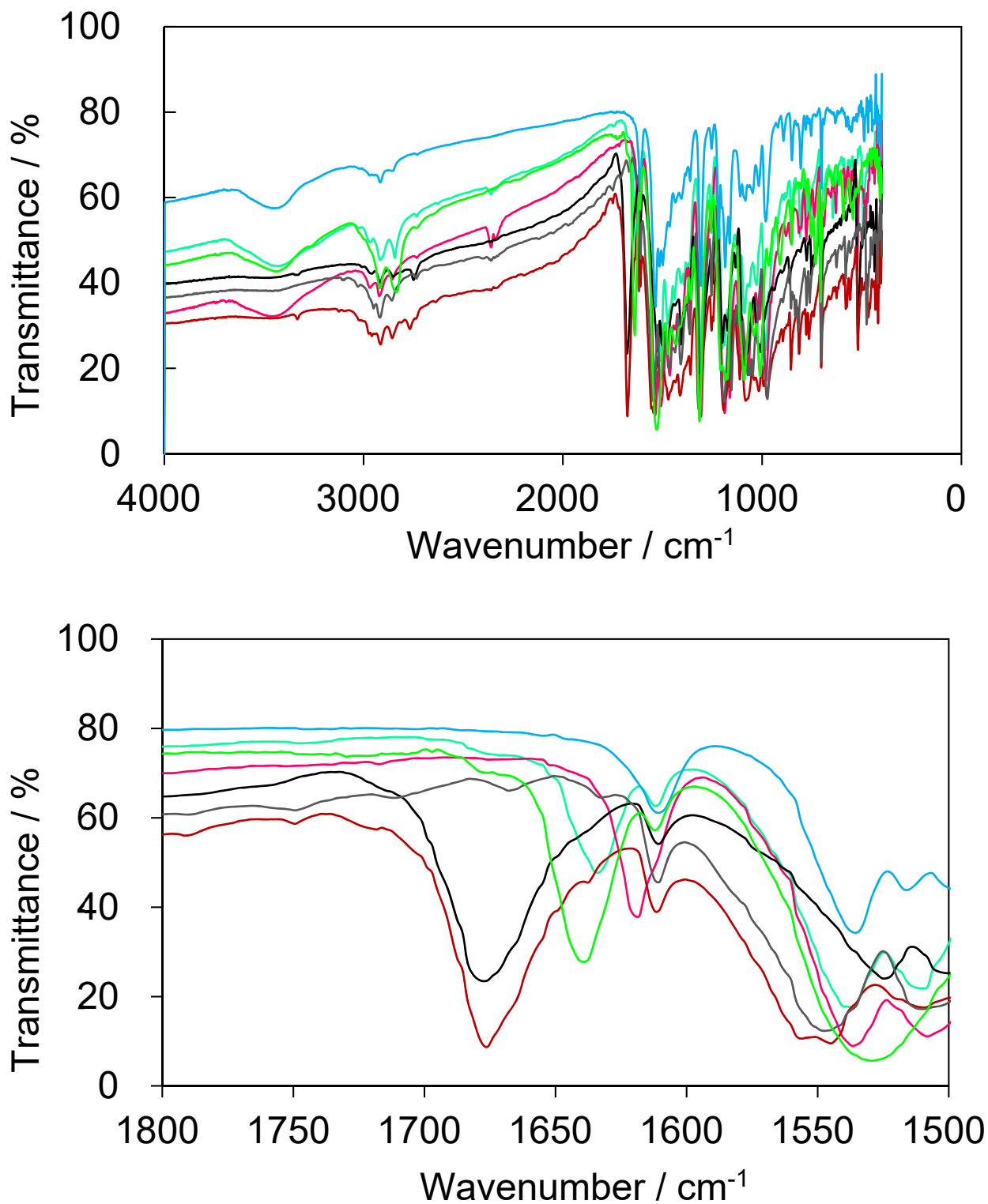


**Fig. S4.** IR spectra of BODIPYs **1** (dark gray), **2** (black), **3** (amber), **6a<sub>2</sub>** (light green), **6c<sub>2</sub>** (pink), **6d<sub>2</sub>** (light blue), and **7a<sub>3-r</sub>** (yellow green) shown for the full region (top) and close-up at the 1500–1800 cm<sup>-1</sup> region (bottom).

### Notes for IR spectroscopy.

IR spectra of **1–3**, **6a<sub>2</sub>**, **6c<sub>2</sub>**, **6d<sub>2</sub>**, and **7a<sub>3-r</sub>** are shown in Figure S4. In the range of 1500 – 1700 cm<sup>-1</sup>, all of the BODIPYs exhibit a signal at 1610 cm<sup>-1</sup>, ascribed to a vibration mode of the BODIPY core. BODIPYs **2** and **3** show strong signals corresponding to C=O stretching at 1676 and 1678 cm<sup>-1</sup>, respectively. Upon reaction with the diamines, the C=O stretching bands vanished and bands corresponding to C=N stretching alternatively appeared at lower wavenumbers in **6a** and **6c**: they display C=N stretching bands at 1633 and 1618 cm<sup>-1</sup>, respectively. As for **6d<sub>2</sub>**, the C=N stretching band is ambiguous because the BODIPY core vibration at 1610 cm<sup>-1</sup> overlaps it. The C=N stretching wavenumbers for **6a<sub>2</sub>**, **6c<sub>2</sub>**, and **6d<sub>2</sub>** are comparable to previous reports.<sup>S9,S10</sup> **7a<sub>3-r</sub>** shows a C=N stretching signal at 1639 cm<sup>-1</sup> without a C=O stretching or primary amine (-NH<sub>2</sub>) stretching signal; this is consistent with the cyclic structure (Scheme 1b), excluding the linear structure with C=O and -NH<sub>2</sub> residues. From IR spectroscopy, the conversion from C=O to C=N was identified.

## E. Thermogravimetric analysis of BODIPYs

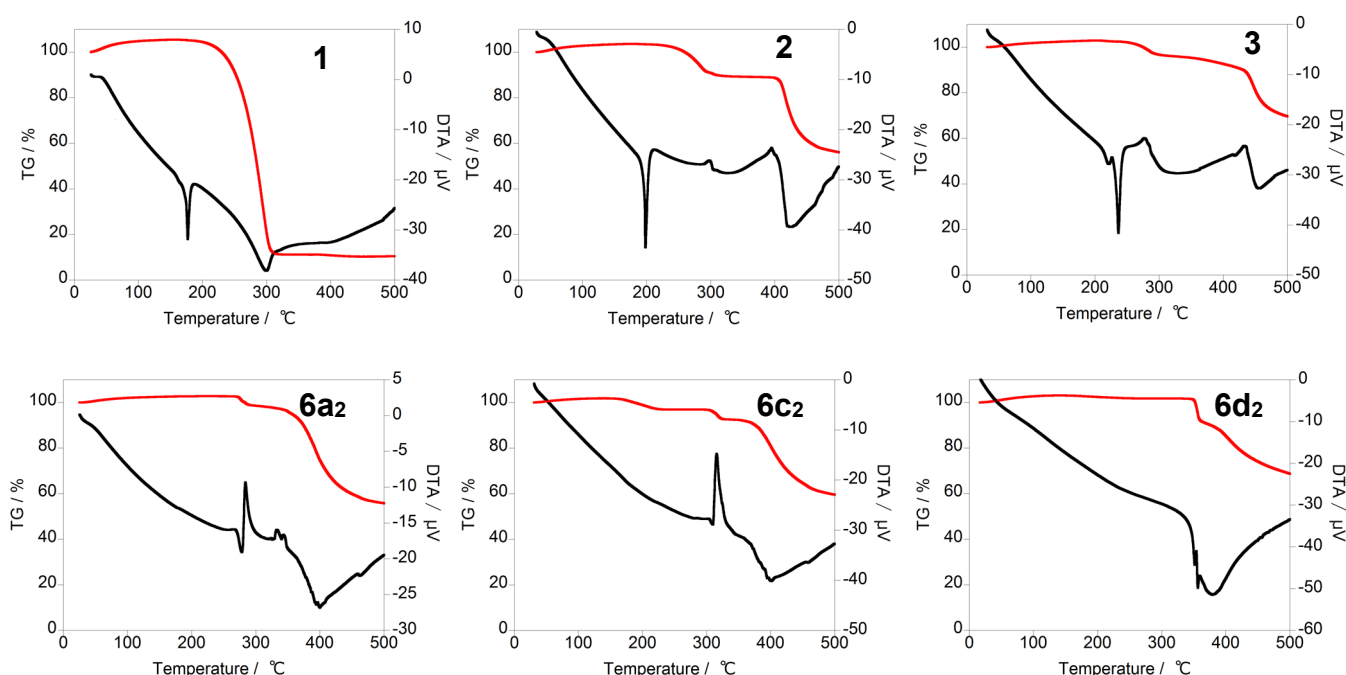


**Fig. S5.** Thermogravimetric (TG) and differential thermal (DT) analysis of BODIPYs **1** – **3**, **6a<sub>2</sub>**, **6c<sub>2</sub>**, and **6d<sub>2</sub>** (red solid line: TG, black solid line: DTA).

**Table S3.** Thermal properties of **1** – **3**, **6a<sub>2</sub>**, **6c<sub>2</sub>**, and **6d<sub>2</sub>**

	m.p. <sup>a</sup> / °C	$T_{\text{decomp}}^{\text{b}}$ / °C	Weight Loss at 500°C / %
<b>1</b>	177	228	89.5
<b>2</b>	197	229	45.6
<b>3</b>	236	238	67.2
<b>6a<sub>2</sub></b>	- <sup>c</sup>	270	44.3
<b>6c<sub>2</sub></b>	- <sup>c</sup>	164	41.7
<b>6d<sub>2</sub></b>	- <sup>c</sup>	350	36.1

<sup>a</sup>Melting point, derived from sharp DTA peak. <sup>b</sup>Temperature at 5% progress of the weight loss by the 1<sup>st</sup> decomposition process. <sup>c</sup>Did not appear before decomposition point.

### Notes for TGA.

Thermogravimetric analysis (TGA) and differential thermal analysis (DTA) of BODIPYs **1**, **2**, **3**, **6a<sub>2</sub>**, **6c<sub>2</sub>**, and **6d<sub>2</sub>** was conducted and summarized in Figure S5 and Table S3. **1** shows stability (5% weight loss of the first decomposition step) up to 228°C, so do **2** and **3** up to 229 and 238°C, respectively. **1** lost 89.5% of

weight at 500°C, while **2** and **3** lost 45.6 % and 67.2 %, respectively. **6a<sub>2</sub>** shows a loss at 270 °C, which is approximately 40°C higher than **2**, boasting improved thermal stability. 44.3% of its weight is lost at 500°C. **6c<sub>2</sub>** starts to decompose at 164°C, presumably due to the relatively weak N–N bond, more susceptible to thermal decomposition. 41.3% of its weight is lost at 500°C. **6d<sub>2</sub>** is even more thermally stable compared to **6a<sub>2</sub>**, whose decomposition starts at 350°C. Thermal analysis on the BODIPYs demonstrated that 1,2-ethylenediimine-linked BODIPY **6a<sub>2</sub>** and 1,4-phenylenediimine-linked BODIPY **6d<sub>2</sub>** displays improved thermal stability compared to **2**.

F. UV/vis spectroscopy and photophysics of BODIPYs

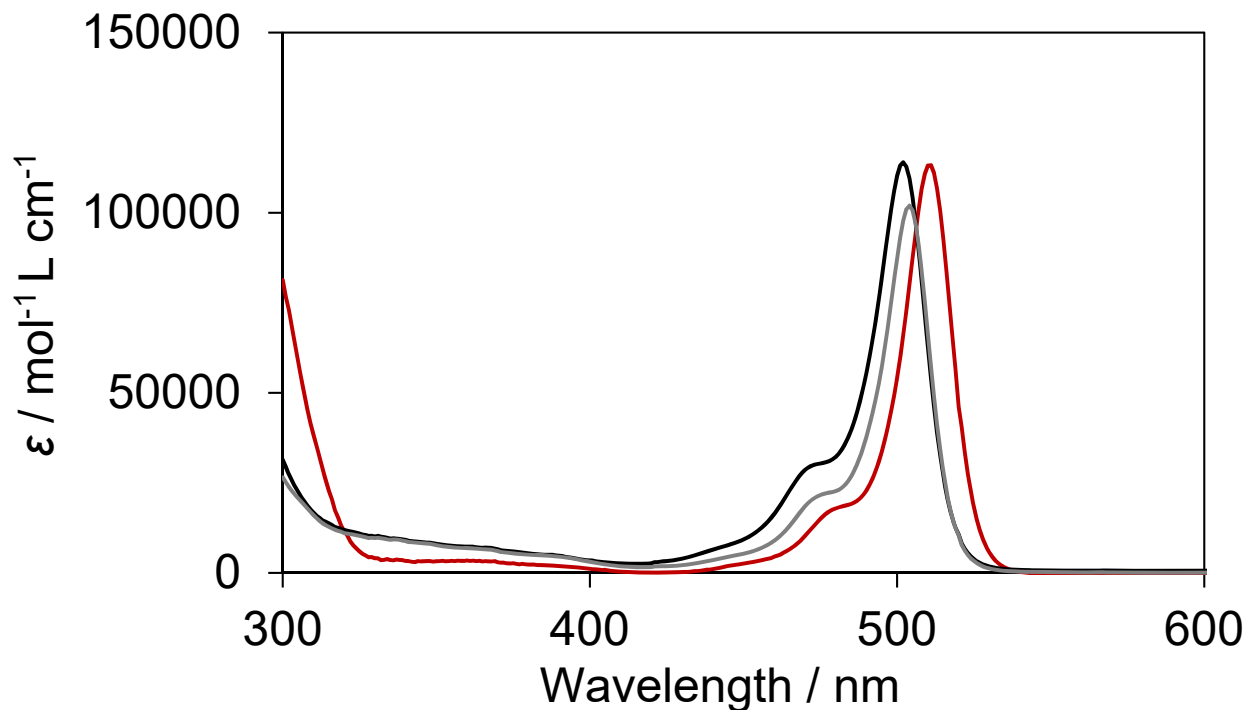


Fig. S6. Absorption spectra of **1** (dark gray), **2** (black), and **3** (amber) in toluene.

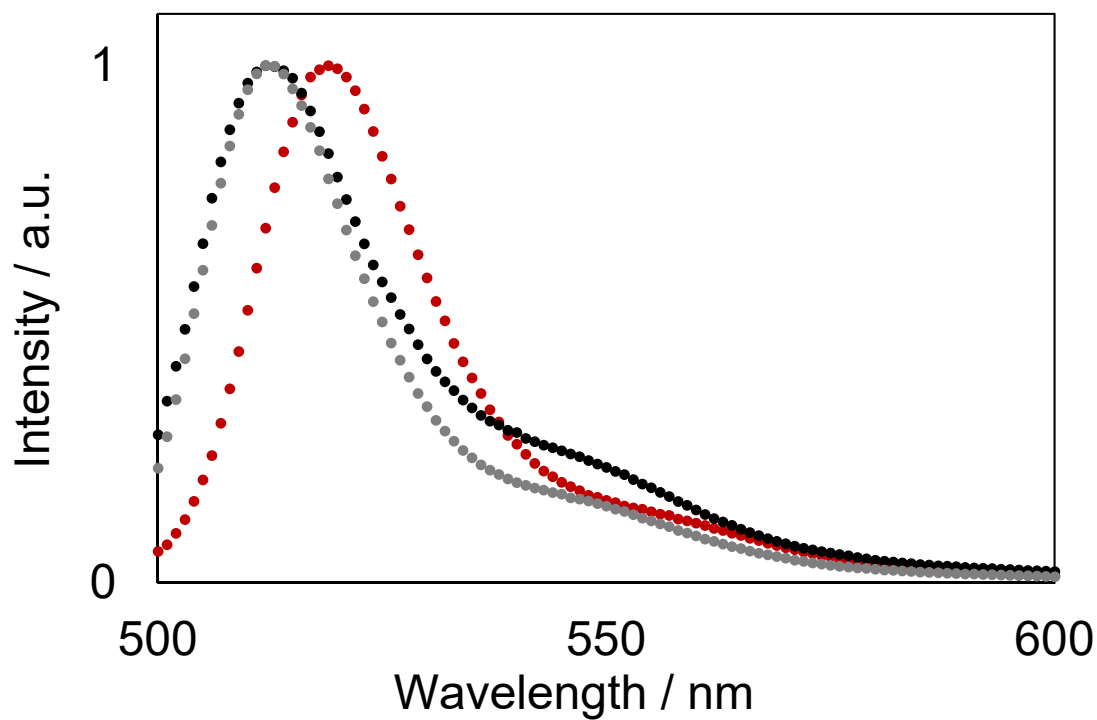
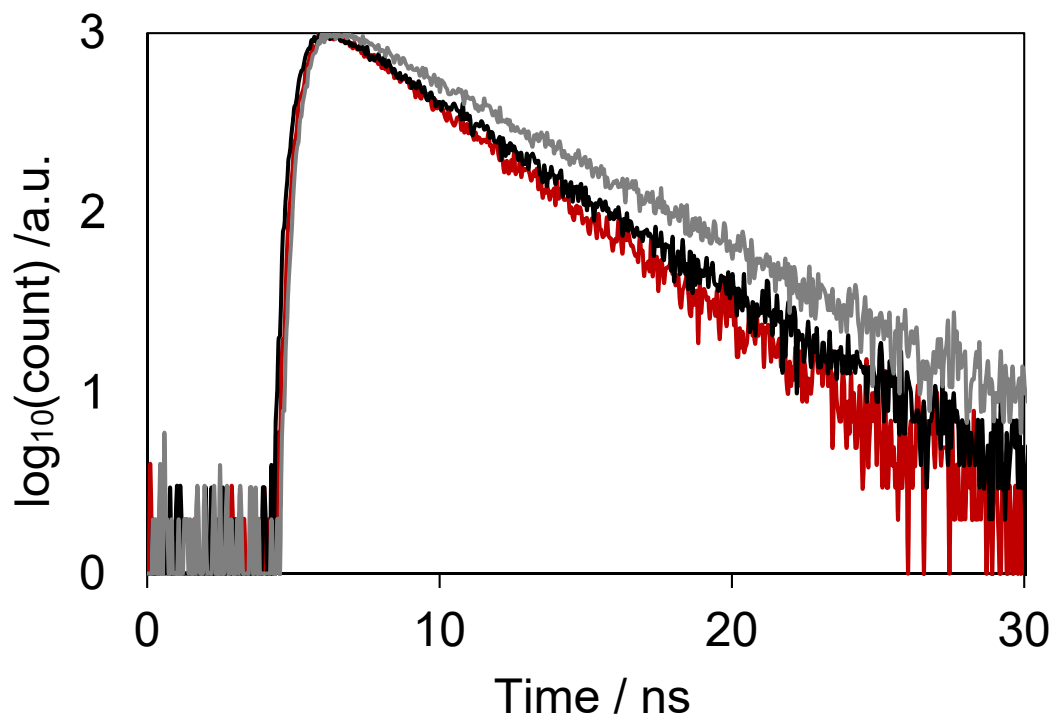
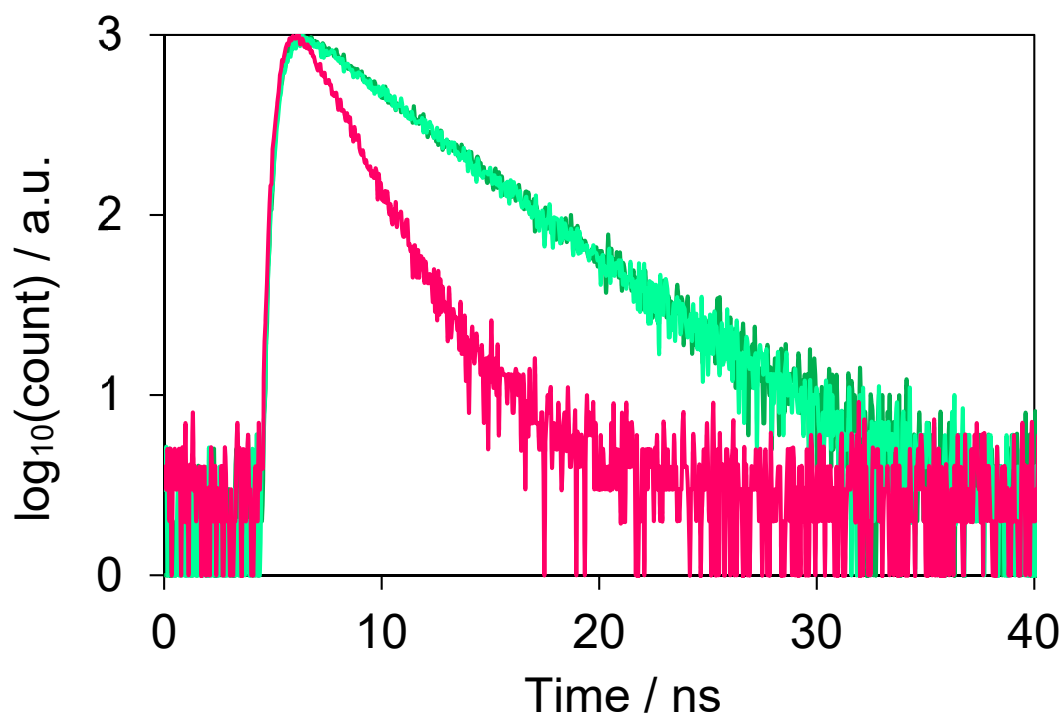


Fig. S7. Emission spectra of **1** (dark gray), **2** (black), and **3** (amber) in toluene.



**Fig. S8.** Fluorescence lifetime decay curves of **1** (dark gray,  $\lambda_{\text{ex}} = 470 \text{ nm}$ ), **2** (black,  $\lambda_{\text{ex}} = 470 \text{ nm}$ ), and **3** (amber,  $\lambda_{\text{ex}} = 470 \text{ nm}$ ).



**Fig. S9.** Fluorescence lifetime decay curves of **6a<sub>2</sub>** (light green,  $\lambda_{\text{ex}} = 470$  nm), **6b<sub>2</sub>** (green,  $\lambda_{\text{ex}} = 470$  nm), and **6c<sub>2</sub>** (magenta,  $\lambda_{\text{ex}} = 590$  nm).

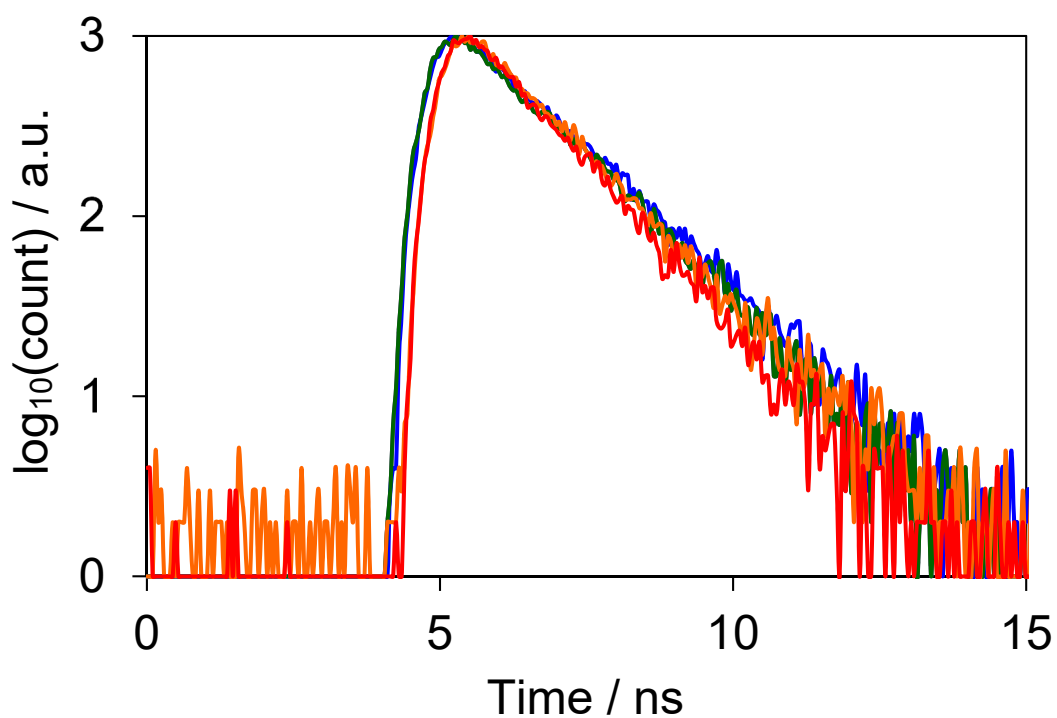


**Fig. S10.** Fluorescence lifetime decay curves of **7c<sub>2</sub>** (purple), **7c<sub>3</sub>** (blue), **7c<sub>4</sub>** (green), **7c<sub>5</sub>** (orange), and **7c<sub>6</sub>** (red).

## G. Electrochemistry

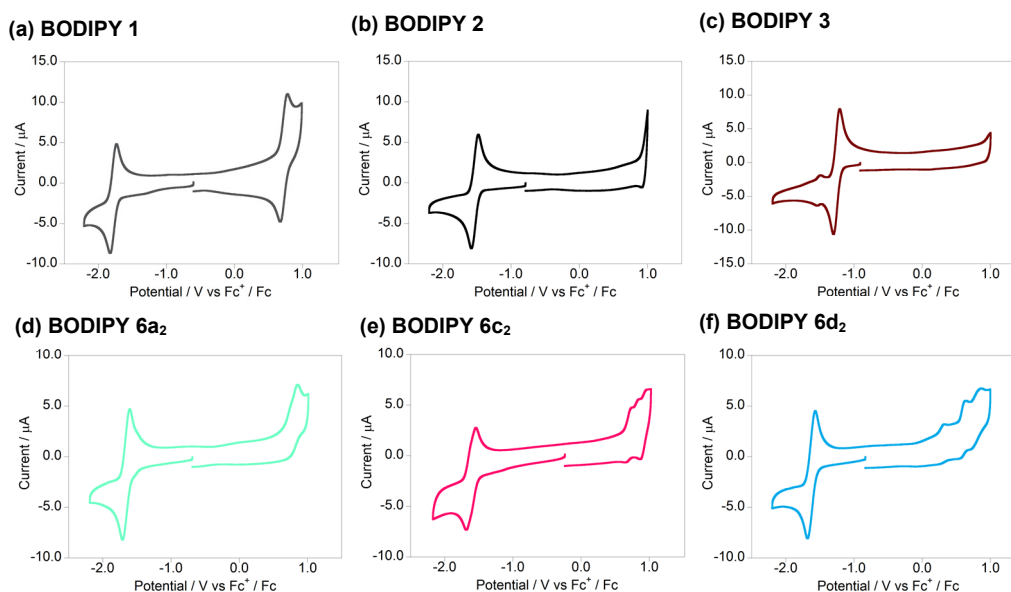


**Fig. S11.** Cyclic voltammograms of BODIPY precursors **1–3** and dimers **6a<sub>2</sub>**, **6c<sub>2</sub>**, **6d<sub>2</sub>** (0.5 mM) in 0.1 M *n*-Bu<sub>4</sub>NPF<sub>6</sub>/dichloromethane. Scan rate = 0.1 V s<sup>-1</sup>. Fc<sup>+</sup>/Fc denotes Ferrocenium/Ferrocene.

**Table S4.** Redox potentials of BODIPY precursors **1–3** and dimers **6a<sub>2</sub>**, **6c<sub>2</sub>**, **6d<sub>2</sub>**

	$E_{\text{red}}^{\text{a}}$ (V)	$E_{\text{ox}}^{\text{b}}$ (V)	$\Delta E^{\text{c}}$ (V)
<b>1</b>	-1.82	0.78	2.60
<b>2</b>	-1.58	N/A <sup>d</sup>	-
<b>3</b>	-1.30	N/A <sup>d</sup>	-
<b>6a<sub>2</sub></b>	-1.71	0.86	2.57
<b>6c<sub>2</sub></b>	-1.68	0.76 <sup>e</sup> , 0.86 <sup>e</sup>	2.44
<b>6d<sub>2</sub></b>	-1.68	0.34, 0.65, 0.88,	2.02

<sup>a</sup>Halfwave potential vs ferrocenium/ferrocene for reductions. <sup>b</sup>Halfwave potential vs ferrocenium/ferrocene for oxidations. <sup>c</sup> $E_{\text{ox}} - E_{\text{red}}$ . <sup>d</sup>Out of the potential window. <sup>e</sup>Shoulder peaks.

### Notes for electrochemical properties.

Electrochemical properties of **1**, **2**, **3**, **6a<sub>2</sub>**, **6c<sub>2</sub>**, and **6d<sub>2</sub>** were obtained by cyclic voltammetry (Figure S11 and Table S4). **1** shows a reversible reduction peak of the BODIPY core at  $E_{\text{red}} = -1.82$  V, consistent with reported analogous structures,<sup>S11</sup> while those of **2** and **3** are -1.58 and -1.30 V, respectively, reflecting the presence of electron-withdrawing formyl groups, shifting the reduction potentials ~0.25 V positively per group. A reversible oxidation wave of the BODIPY core is observed at 0.78 V in **1**, though those of **2** and **3** were out of the potential window because of the positive shift.

**6a<sub>2</sub>** shows a reversible reduction wave at -1.71 V and an irreversible oxidation wave at 0.86 V. The conversion of the formyl groups to imino groups shifted the reduction potential negatively by 0.13 V, compared to that of **2**. Dimer **6c<sub>2</sub>** shows a reversible reduction wave at -1.68 V, with three irreversible oxidation waves at 0.76 and 0.86 V. The redox gap is narrower in **6c<sub>2</sub>**, in agreement with its bathochromically shifted absorption and fluorescence spectra compared to those of **6a<sub>2</sub>**. Dimer **6d<sub>2</sub>** exhibits a reversible reduction wave at -1.68 V and three irreversible oxidation waves at 0.34, 0.65, 0.88 V. The first oxidation peak is attributed to the electron-rich phenylene diamine subunit, while the latter peaks can be assigned to oxidation waves of one BODIPY core subunits and the other unit.

## H. DFT calculation

**Table S5.** Energy levels of selected molecular orbitals in **1**, **2**, and **3** (values shown in eV versus vacuum level)

	<b>1</b>	<b>2</b>	<b>3</b>
LUMO+2	1.51	0.66	-1.14
LUMO+1	0.93	-0.91	-1.28
LUMO	-2.42	-2.82	-3.21
HOMO	-5.38	-5.83	-6.23
HOMO-1	-6.56	-6.64	-6.93
HOMO-2	-6.74	-6.86	-6.97

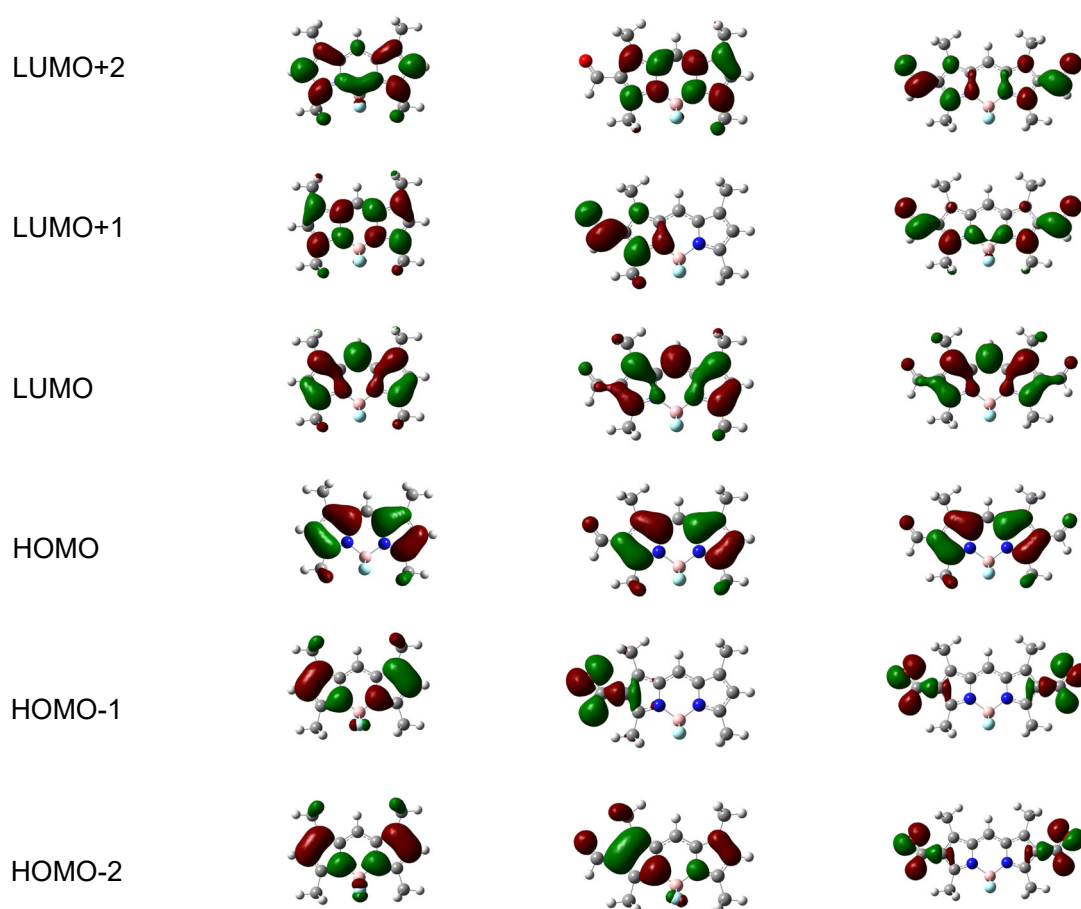


**Fig. S12.** Diagrams of selected frontier molecular orbitals for **1** (left), **2** (center), and **3** (right) by DFT at the B3LYP/6-31G(d) level (Isovalue = 0.03).

**Table S6.** Energy levels of selected molecular orbitals in **6a<sub>2</sub>**, **6c<sub>2</sub>**, and **6d<sub>2</sub>** (values shown in eV versus vacuum level)

	<b>6a<sub>2</sub></b>	<b>6c<sub>2</sub></b>	<b>6d<sub>2</sub></b>
LUMO+2	-0.54	-1.14	-1.39
LUMO+1	-2.57	-2.55	-2.68
LUMO	-2.58	-2.67	-2.73
HOMO	-5.49	-5.25	-5.19
HOMO-1	-5.54	-5.67	-5.61
HOMO-2	-6.29	-6.05	-5.82

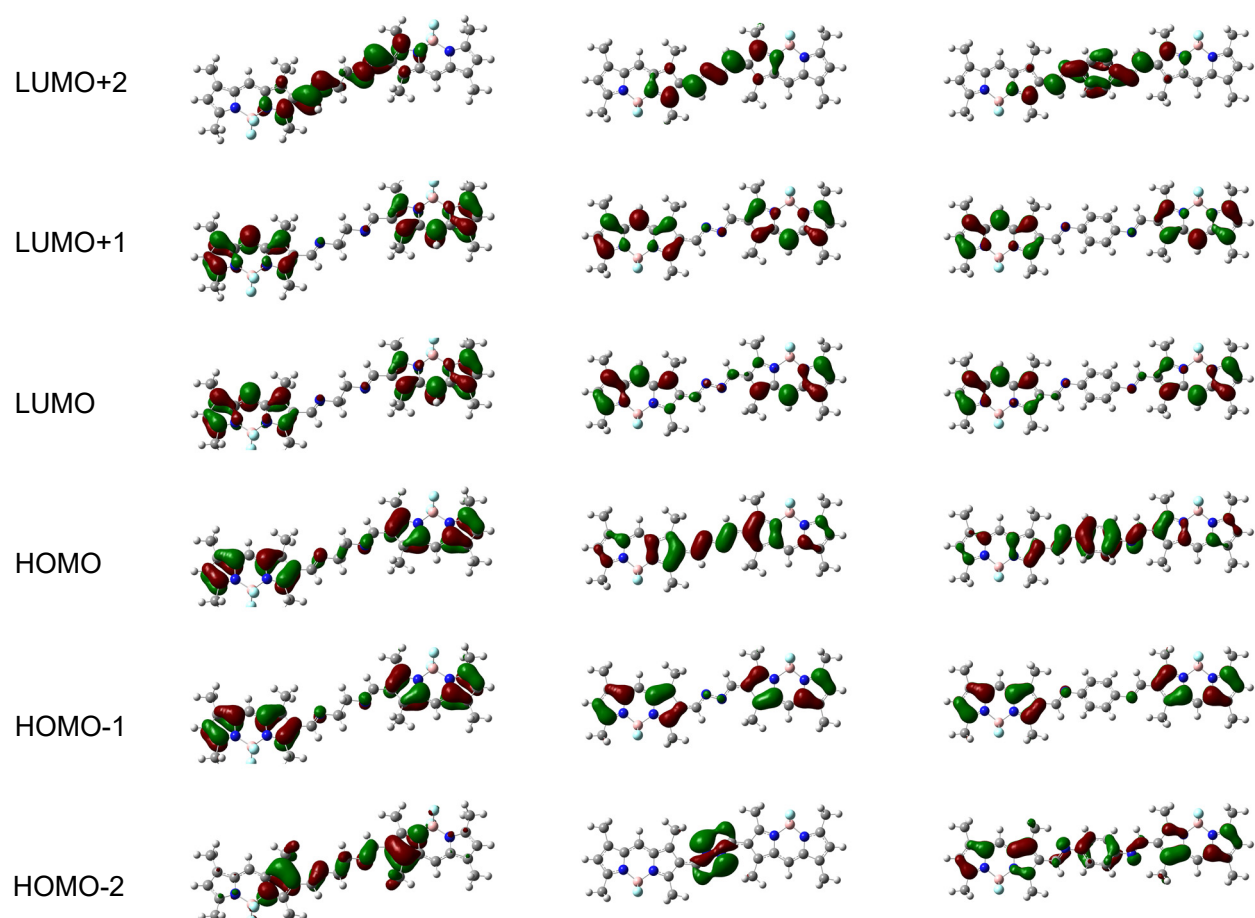


**Fig. S13.** Diagrams of selected frontier molecular orbitals for **6a<sub>2</sub>** (left), **6c<sub>2</sub>** (center), and **6d<sub>2</sub>** (right) by DFT at the B3LYP/6-31G(d) level (Isovalue = 0.03).

**Table S7.** Energy levels of selected molecular orbitals in  $7c_2$ ,  $7c_3$ , and  $7c_4$  (values shown in eV versus vacuum level).

	$7c_2$	$7c_3$	$7c_4$
LUMO+2	-1.56	-2.90	-2.95
LUMO+1	-3.00	-3.03	-3.05
LUMO	-3.14	-3.11	-3.09
HOMO	-5.73	-5.55	-5.46
HOMO-1	-6.14	-5.84	-5.66
HOMO-2	-6.50	-6.10	-5.89

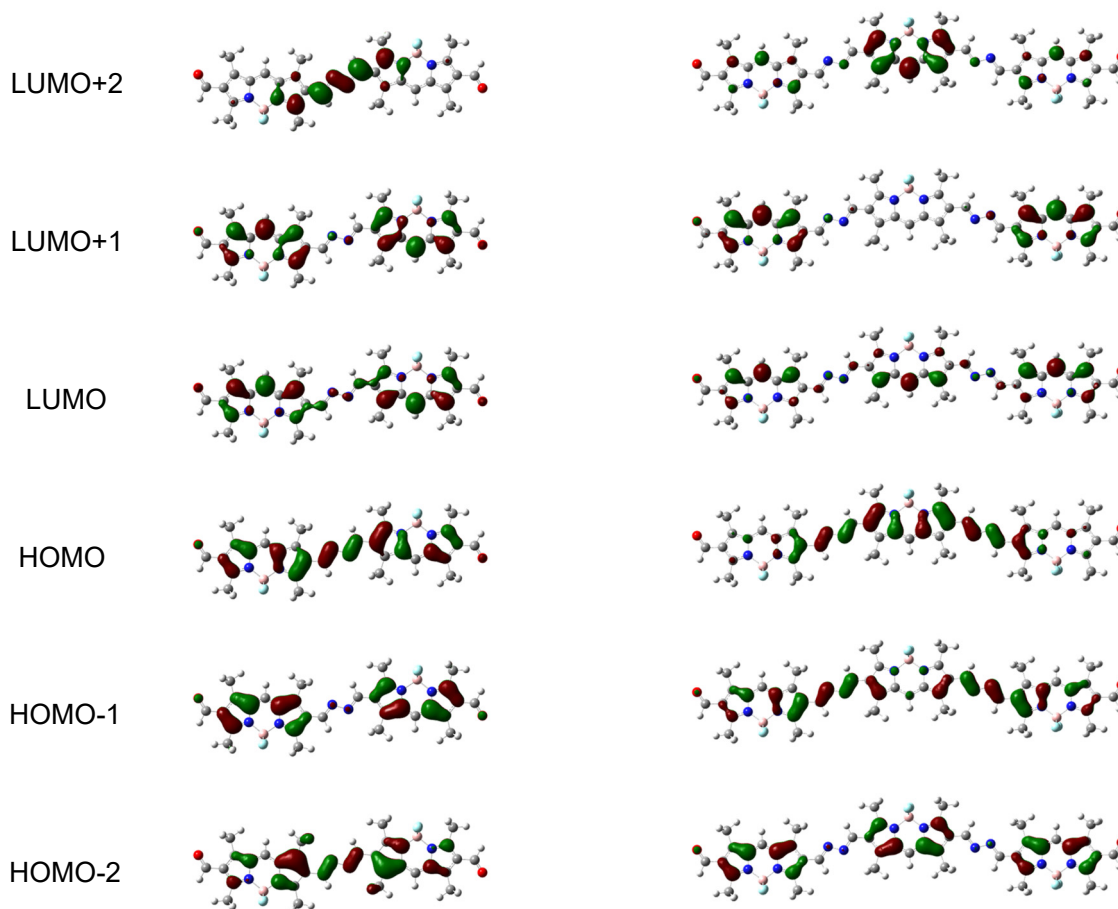


**Fig. S14.** Diagrams of selected frontier molecular orbitals for  $7c_2$  (left) and  $7c_3$  (right) by DFT at the B3LYP/6-31G(d) level (Isovalue = 0.03).

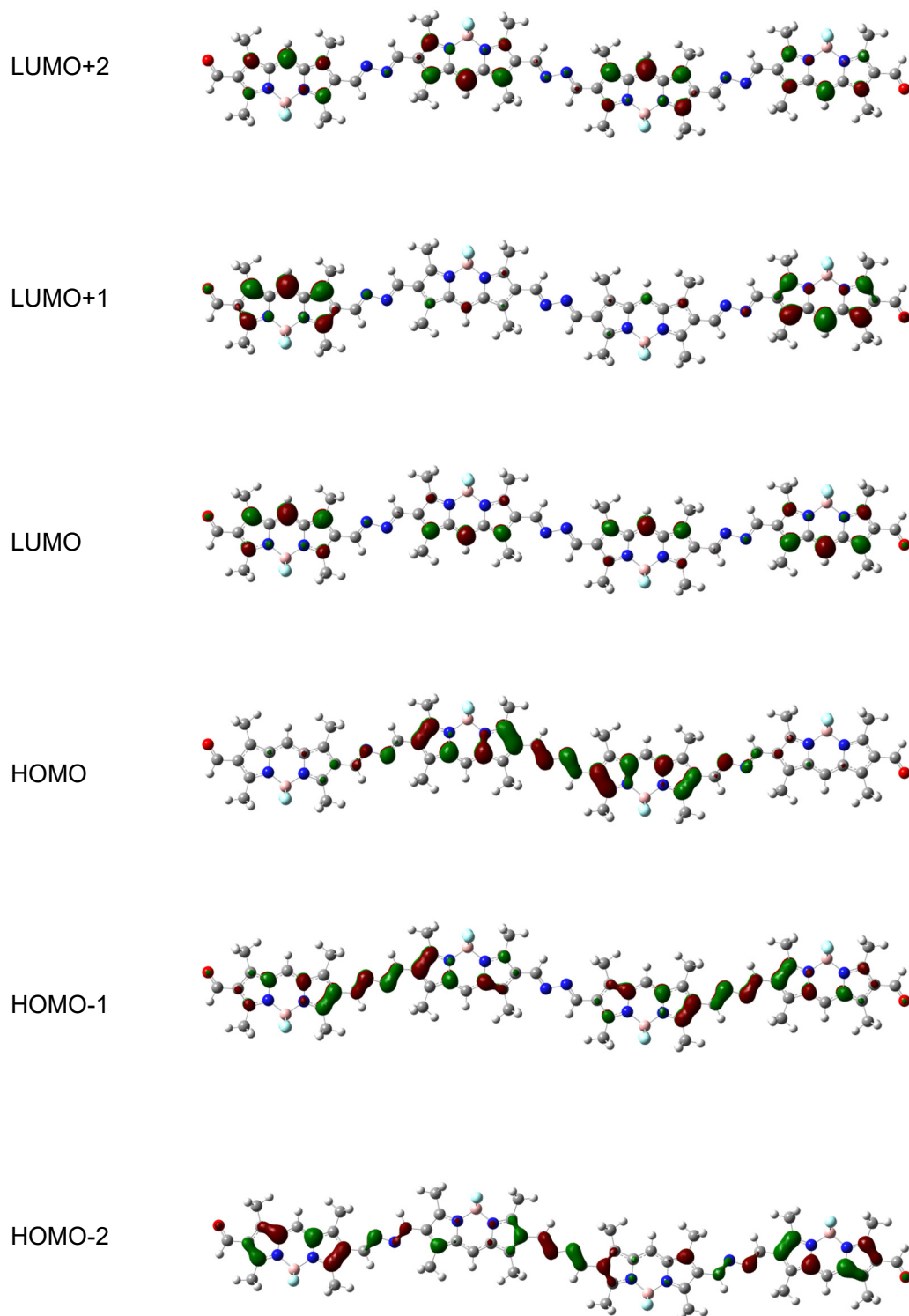


**Fig. S15.** Diagrams of selected frontier molecular orbitals for  $7c_4$  by DFT at the B3LYP/6-31G(d) level (Isovalue = 0.03).

### Notes for DFT calculation.

The electronic structure of BODIPYs **1**, **2**, **3**, **6a<sub>2</sub>**, **6c<sub>2</sub>**, **6d<sub>2</sub>** were further investigated using density functional theory (DFT) calculation (Fig. S12–S15 and Tables S5–S7). The calculations of **1–3** showed that their HOMOs and LUMOs are on the BODIPY core, whose shape and distribution are shared by the three BODIPYs. The energy levels of the HOMOs of **1–3** are -5.38, -5.83, and -6.23 eV (versus vacuum level, Figure S12 and Table S5), respectively, showing stabilization of approximately 0.4 eV per one formyl group. Their LUMOs exhibited the same trend, whose energy levels are -2.42, -2.82, and -3.21 eV, respectively. This is comparable to their electrochemical results, whose reduction potentials ( $E_{\text{red}}$ ) positively shift as the number of formyl groups increases (Table S4). Their HOMO–LUMO gaps are 2.96, 3.01, and 3.02 eV, virtually constant, consistent with the negligible difference in their absorption and emission maxima (Figure 2 and Table 1). **6a<sub>2</sub>**'s orbitals comprise virtually degenerate HOMO-1 (-5.54 eV) and HOMO (-5.49 eV), and LUMO (-2.58 eV) and LUMO+1 (-2.57 eV), corresponding to the  $\pi$  and  $\pi^*$  orbitals of the two independent BODIPY cores, respectively (Figure S13 and Table S6). **6a<sub>2</sub>**'s HOMO and LUMO are elevated by 0.34 and 0.24 eV compared to those of **2**, respectively; the elevated LUMO agrees with its electrochemical results, whose reduction potential is negatively shifted compared to that of **2** (Table S4). On the contrary, **6c<sub>2</sub>**'s calculation shows that there are greater energy gaps between HOMO (-5.25 eV) and HOMO-1 (-5.67 eV), and LUMO (-2.67 eV) and LUMO+1 (-2.55 eV) than those in **6a<sub>2</sub>**. These results indicate that the  $\pi$ -conjugation in **6c<sub>2</sub>** delocalizes over the two BODIPY units through the azine bridge, while that in **6a<sub>2</sub>** is not effective. The calculated HOMO–LUMO gap in **6c<sub>2</sub>** (2.58 eV) is narrower than that obtained for **6a<sub>2</sub>** (2.91 eV). This is consistent with their UV-vis absorption and emission spectra, since those of **6c<sub>2</sub>** is 30 – 50 nm red-shifted compared to those of **6a<sub>2</sub>** (Figure 2 and Table 1). Similarly, **6d<sub>2</sub>**'s calculated electronic structure reveals that the frontier orbitals are delocalized over the two BODIPY units, however, the HOMO (-5.19 eV) is chiefly contributed by the phenylenediimine bridge. We also conducted DFT calculation for **7c<sub>2</sub>**, **7c<sub>3</sub>**, and **7c<sub>4</sub>** (Figures S14, S15 and Table S7). As **6c<sub>2</sub>**, the oligomers also possess HOMOs and LUMOs delocalized over their BODIPY units via the azine bridge. The HOMO–LUMO gaps of **7c<sub>2</sub>**, **7c<sub>3</sub>**, and **7c<sub>4</sub>** were calculated to be 2.59, 2.44, and 2.37 eV, respectively, narrower than that of **3** (3.02 eV), in agreement with the red-shifting trend of the three oligomers in their UV-vis absorption and emission spectra. Overall, DFT calculations have revealed that the frontier orbitals of the azine-bridged BODIPYs are delocalized through  $\pi$ -conjugation, whose HOMO–LUMO gaps narrow as the number of the BODIPY units increases.

## I. Photophysical properties of BODIPY-loaded silica gel

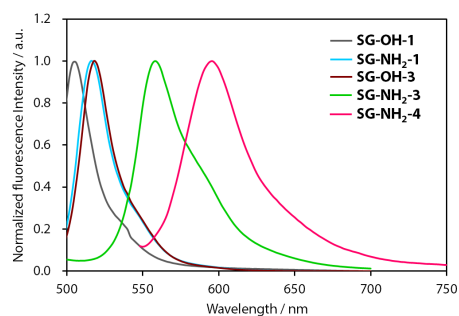


**Fig. S16.** Normalized fluorescence spectra of BODIPY-loaded silica gel samples.

**Table S8.** Photophysical properties of BODIPY-loaded silica gel samples

	$\lambda_{fl}(\lambda_{ex})^a$ (nm)	$\phi_F^b$	$\tau^c$ (ns)
<b>SG-OH-1</b>	506 (450)	0.58	9.0
<b>SG-NH<sub>2</sub>-1</b>	516 (450)	0.56	8.8
<b>SG-OH-3</b>	518 (450)	0.57	6.4
<b>SG-NH<sub>2</sub>-3</b>	558 (450)	0.64	6.5
<b>SG-NH<sub>2</sub>-4</b>	596 (520)	0.50	4.2

<sup>a</sup>Fluorescence wavelength ( $\lambda_{fl}$ ) excited at excitation wavelength ( $\lambda_{ex}$ ). <sup>b</sup>Fluorescence quantum yield. <sup>c</sup>Fluorescence lifetime.

## J. References for SI

- S1 N. Sakamoto, C. Ikeda, M. Yamamura and T. Nabeshima, *Chem. Commun.*, 2012, **48**, 4818–4820.
- S2 Y. Rong, C. Wu, J. Yu, X. Zhang, F. Ye, M. Zeigler, M. E. Gallina, I. C. Wu, Y. Zhang, Y. H. Chan, W. Sun, K. Uvdal and D. T. Chiu, *ACS Nano*, 2013, **7**, 376–384.
- S3 E. Angeletti, C. Canepa, G. Martinetti and P. Venturello, *J. Chem. Soc. Perkin Trans.*, 1989, **1**, 105–107.
- S4 K. Sugimoto, H. Ohsumi, S. Aoyagi, E. Nishibori, C. Moriyoshi, Y. Kuroiwa, H. Sawa, M. Takata, R. Garrett, I. Gentle, K. Nugent and S. Wilkins, *AIP Conference Proceedings*, 2010, **1234**, 887–890.
- S5 (a) A. Altomare, G. Cascarano, C. Giacovazzo, A. Guagliardi, M.C. Burla, G. Polidori and M. S. Camalli, *J. Appl. Cryst.*, 1994, **27**, 435; (b) M. C. Burla, R. Caliandro, M. Camalli, B. Carrozzini, G. L. Cascarano, L. De Caro, C. Giacovazzo, G. Polidori and R. Spagna, *J. Appl. Cryst.*, 2005, **38**, 381–388; (c) G. M. Sheldrick, *Acta Cryst.*, 2008, **A64**, 112–122.
- S6 S. G. Awuah and Y. You, *RSC Adv.*, 2012, **2**, 11169–11183.
- S7 (a) S. Kusaka, R. Sakamoto, Y. Kitagawa, M. Okumura and H. Nishihara, *Chem. Asian J.*, 2013, **8**, 723–727; (b) P. E. Kesavan, S. Das, M. Y. Lone, P. C. Jha, S. Mori, I. Gupta, *Dalton Trans.*, 2015, **44**, 17209–17221.
- S8 V. R. Vangala, A. Nangia and V. M. Lynch, *Chem. Commun.*, 2002, **12**, 1304–1305; (b) A. B. Souza, M. A. R. C. Alencar, S. H. Cardoso, M. S. Valle, R. Diniz, J. M. Hickmann, *Opt. Mater.*, 2013, **35**, 2535–2539; (c) M. Ghazzali, V. Langer, C. Lopes, A. Eriksson and L. Öhrström, *New J. Chem.*, 2007, **31**, 1777–1784.
- S9 J. E. Kovacic, *Spectrochim. Acta Part A Mol. Spectrosc.*, 1967, **23**, 183–187.
- S10 (a) M. Abo Aly, *Spectrochim. Acta Part A Mol. Biomol. Spectrosc.*, 1999, **55**, 1711–1714; (b) R. A. Nyquist, T. L. Peters and P. B. Budde, *Spectrochim. Acta Part A Mol. Spectrosc.*, 1978, **34**, 503–504; (c) N. Subramanian, N. Sundaraganesan and J. Jayabharathi, *Spectrochim. Acta Part A Mol. Biomol. Spectrosc.*, 2010, **76**, 259–269; (d) J. E. Kovacic, *Spectrochim. Acta Part A Mol. Spectrosc.*, 1967, **23**, 183–187.
- S11 (a) A. Burghart, H. Kim, M. B. Welch, L. H. Thoresen, J. Reibenspies, K. Burgess, F. Bergström and L. B.-Å. Johansson, *J. Org. Chem.*, 1999, **64**, 7813–7819; (b) A. Poirel, A. De Nicola, P. Retailleau and R. Ziessel, *J. Org. Chem.*, 2012, **77**, 7512–7525.